

# Surface Density Function and its evolution in Homogeneous and Inhomogeneous n-heptane MILD Combustion

K. Abo-Amsha, N. Chakraborty  
School of Engineering, Newcastle University, Newcastle Upon Tyne  
NE1 7RU, United Kingdom

## 1 Introduction

As the environmental regulations become more and more stringent, a new generation of highly efficient and environmentally friendly combustion techniques are required. In this context, Moderate or Intense Low Oxygen Dilution (MILD) combustion has emerged as a novel concept with both high-energy efficiency and ultra-low emission potentials [1]. In MILD combustion, the fuel-air mixture is preheated above its autoignition temperature ( $T_r > T_{ign}$ ), while the maximum temperature rise remains smaller than the autoignition temperature ( $\Delta T|_{\max} < T_{ign}$ ) [1]. This can be achieved by recirculating the hot flue gas in furnaces and boilers, which inherently increases their thermal efficiency. Experimental investigations of MILD combustion demonstrated the presence of flame fronts, but indications of distributed burning were revealed through temperature measurements [2, 3]. Minamoto and co-workers conducted 3D DNS studies of Exhaust Gas Recirculation (EGR) type, homogeneous mixture, MILD combustion, where they investigated the distribution of species, temperature, and reaction rate fields and concluded that the distributed combustion seen in experimental visualisation [2, 3] can be attributed to the interaction of thin reaction zones [4]. Ahn-Khoa and co-workers extended the previous analysis for stratified mixture (Inhomogeneous) MILD combustion and provided important insights into the flame structure, reaction zone topology and markers of combustion mode [5]. These DNS analyses [4, 5] revealed that the convolution of the reaction zones in MILD combustion is strongly influenced by the dilution factor of the reacting mixture as well as the turbulence-chemistry interaction. Recent studies using DNS data indicated that flamelet-based models can be applied to gaseous fuel MILD combustion with some modifications [4, 6]. However, when applied to MILD combustion in Reynolds Averaged Navier-Stokes (RANS) and Large Eddy Simulations (LES) type investigations, the conventional flamelet and eddy dissipation approaches provided good agreement with experimental data in terms of mean velocity and temperature fields, but discrepancies have been reported in terms of peak temperature and minor species concentrations [7, 8]. Thus, further investigations are needed to fully understand the behaviour of flamelet-based approaches in MILD combustion. In this context, the natural first step is to investigate the statistical behaviour of the magnitude of the gradient of the reaction progress variable (Surface Density Function (SDF)  $= |\nabla c|$ ) since it is closely related to the Scalar Dissipation Rate (SDR) ( $N_c = D_c |\nabla c|^2$  with  $D_c$  being the reaction progress variable diffusivity) and generalised Flame Surface Density (FSD) ( $\Sigma_{gen} = |\overline{\nabla c}|$  with the overbar suggesting a Reynolds averaging/LES filtering operation as appropriate). Particularly, it is important to understand the influence of the strain rates induced by fluid motion and flame propagation on the SDF evolution in homogeneous and inhomogeneous mixture MILD combustion. The present analysis aims to address this gap in the literature by conducting three dimensional DNS with reduced n-heptane/air chemical mechanism for EGR type homogeneous and inhomogeneous mixture MILD combustion and at two dilution levels ( $X_{O_2} = 4.5\%, 3.0\%$ ). The main

objectives of the current analysis are: 1. A comparison between the SDF statistics in EGR-type homogeneous and inhomogeneous mixture MILD combustion 2. Highlighting the effect of oxygen dilution levels on SDF statistics.

## 2 Mathematical Background

The reaction progress variable ( $c$ ) is used to quantify the extent of reaction completion. In this work,  $c$  has been defined based on the oxidiser mass fraction ( $Y_{O_2}$ ) as follows:

$$c = \frac{(1 - \xi)Y_{O_2,2} - Y_{O_2}}{(1 - \xi)Y_{O_2,2} - \max\left[0, \frac{\xi_{st} - \xi}{\xi_{st}} Y_{O_2,2}\right]} \quad (1)$$

where  $Y_{O_2,2}$  is the oxidiser mass fraction in the oxidiser stream, while  $\xi$  and  $\xi_{st}$  are the mixture fraction and the stoichiometric mixture fraction, respectively. The choice of oxygen as the progress variable species is justified since larger hydrocarbons, like n-heptane, tend to breakdown to smaller ones at high temperatures. Thus defining the progress variable based on fuel will be less representative of the whole combustion process. Moreover, the Lewis number ( $Le$ ) value of 1.11 for oxygen, makes it more suitable for this analysis than n-heptane ( $Le = 3.0$ ). Following Bilger [9], both  $\xi$  and  $\xi_{st}$  were defined in terms of the elemental mass fractions and atomic masses as  $\xi = (\beta - \beta_2)/(\beta_1 - \beta_2)$  and  $\xi_{st} = -\beta_2/(\beta_1 - \beta_2)$  where  $\beta = 2Z_c/W_c + 0.5Z_H/W_H - Z_O/W_O$ ,  $Z_j$  and  $W_j$  are the elemental mass fractions and atomic masses for carbon, oxygen and hydrogen atoms. The subscripts 1, 2 refer to the fuel and (diluted) oxidiser streams, respectively. A transport equation for the reaction progress variable can be written as:

$$\rho \frac{\partial c}{\partial t} + \rho u_j \frac{\partial c}{\partial x_j} = \frac{\partial}{\partial x_j} \left( \rho D_c \frac{\partial c}{\partial x_j} \right) + \dot{w}_c + A_\xi \quad (2)$$

where  $\rho$  is the gas density,  $D_c$  is the mass diffusivity of the species on which the progress variable is based,  $u_j$  is the  $j^{th}$  velocity component,  $\dot{w}_c$  is the reaction rate of the progress variable and  $A_\xi$  arises due to  $\xi$  gradient. Both  $\dot{w}_c$  and  $A_\xi$  are expressed as functions of  $\xi$  and  $Y_{O_2,2}$  as follows:

$$\dot{w}_c = -\xi_{st} \dot{w}_{O_2} / [Y_{O_2,2} \xi (1 - \xi_{st})] \text{ for } \xi \leq \xi_{st}; \quad \dot{w}_c = -\dot{w}_{O_2} / [Y_{O_2,2} (1 - \xi)] \text{ for } \xi > \xi_{st} \quad (3)$$

$$A_\xi = 2\rho D_c \nabla \xi \cdot \nabla c / \xi \text{ for } \xi \leq \xi_{st}; \quad A_\xi = -2\rho D_c \nabla \xi \cdot \nabla c / (1 - \xi) \text{ for } \xi > \xi_{st} \quad (4)$$

For a given  $c$  iso-surface, Eq. (2) can be rewritten as [10]  $\partial c / \partial t + u_j \partial c / \partial x_j = S_d |\nabla c|$  where  $S_d$  is the displacement speed of the given  $c$  iso-surface and is given by:  $S_d = [\dot{w}_c + \nabla \cdot (\rho D_c \nabla c) + A_\xi] / \rho |\nabla c|$ . The displacement speed can be written in terms of its components as follows:  $S_d = S_r + S_n + S_t + S_\xi$  where  $S_r$ ,  $S_n$ ,  $S_t$  and  $S_\xi$  are the reaction, normal and tangential diffusion and mixture inhomogeneity components of  $S_d$ , respectively. These components are defined as [10]:

$$S_r = \dot{w}_c / (\rho |\nabla c|), \quad S_n = \vec{N} \cdot \nabla (\rho D_c \vec{N} \cdot \nabla c) / (\rho |\nabla c|), \quad S_t = -2D_c \kappa_m, \quad S_\xi = A_\xi / (\rho |\nabla c|), \quad (5)$$

where  $\vec{N} = -\nabla c / |\nabla c|$  is the flame normal vector and  $\kappa_m = 0.5 \nabla \cdot \vec{N}$  is the flame curvature. The kinematic form of the reaction progress variable equation can be used to obtain a transport equation for the Surface Density Function (SDF =  $|\nabla c|$ ) at a given  $c$  iso-surface can be written as [11]:

$$\partial |\nabla c| / \partial t + \partial (u_j |\nabla c|) / \partial x_j = a_T |\nabla c| - \partial (S_d N_j |\nabla c|) / \partial x_j + 2S_d \kappa_m |\nabla c| \quad (6)$$

where  $a_T = (\delta_{ij} - N_i N_j) \partial u_i / \partial x_j$  is the tangential strain rate,  $-\partial (S_d N_j |\nabla c|) / \partial x_j$  is the SDF propagation term and  $2S_d \kappa_m |\nabla c|$  is the SDF curvature term. Eq. (6) can be rewritten in a reference frame attached to the flame as follows [11]:

$$(1/|\nabla c|) d|\nabla c|/dt = -(1/\Delta x_N) d\Delta x_N/dt = -a_N - N_j \partial S_d / \partial x_j = -a_N^{eff} \quad (7)$$

where  $d(\dots)/dt = \partial(\dots)/\partial t + V_j^c \partial(\dots)/\partial x_j$  is the total derivative in the reference frame attached to the flame,  $V_j^c = u_j + S_d N_j$  is the  $j^{\text{th}}$  component of the flame propagation velocity,  $\Delta x_N$  is the distance between two adjacent  $c$  iso-surfaces. The effective normal strain rate  $a_N^{\text{eff}}$  has contributions from the fluid dynamic normal strain rate  $a_N$  and the normal strain rate due to flame propagation  $N_j \partial S_d / \partial x_j$ . It is also worthwhile to investigate the evolution of the elemental reaction zone surface area ( $\delta A$ ) since it is closely related to  $|\nabla c|$  (i.e.  $A = \int_V |\nabla c| dV$ ). The transport equation for  $\delta A$  is given by [11]:

$$(1/\delta A) d(\delta A)/dt = a_T + 2S_d \kappa_m = a_T^{\text{eff}} \quad (8)$$

where  $a_T^{\text{eff}}$  is the effective tangential strain rate,  $a_T$  is the fluid dynamic tangential strain rate, and  $2S_d \kappa_m$  arises due to flame propagation.

From the previous presentation, it is evident that  $a_N$ ,  $a_T$ ,  $2S_d \kappa_m$ ,  $N_j \partial S_d / \partial x_j$ ,  $a_N^{\text{eff}}$  and  $a_T^{\text{eff}}$  drive the statistical behaviours of SDF and  $\delta A$ . Thus, these strain rates will be discussed in this work.

### 3 Numerical Implementation

For the current study, the compressible DNS code SENG2 [4] has been used. In this code, the standard conservation equations of mass, momentum, energy and species mass fractions for compressible reacting flows are solved in dimensional form with the thermo-physical properties such as viscosity, thermal conductivity, specific heat capacities and mass diffusivities taken to be temperature dependent. The SENG2 code employs a 10<sup>th</sup> order central difference scheme for spatial differentiation at the internal grid points, but the order of accuracy gradually reduces to a one-sided fourth-order scheme at the non-periodic boundaries. A fourth-order explicit low storage Runge-Kutta scheme is used for time advancement. The boundary conditions are specified according to the Navier-Stokes Characteristic Boundary Condition (NSCBC) methodology. A reduced chemical mechanism comprising 22 species and 18-steps has been taken to represent the chemical kinetics of combustion [12].

A cubic domain with an edge  $L = 20 \text{ mm}$  is discretised by a Cartesian grid with uniform spacing comprising of 216 nodes in each direction. The resulting grid spacing ensures that both the thermal flame thickness ( $\delta_{th} = (T_p - T_r) / \max |\nabla T|_L$  where  $T$ ,  $T_p$  and  $T_r$  are the instantaneous, products and reactants temperatures and the subscript  $L$  refers to the 1D unstretched laminar flame) and the Kolmogorov length scale ( $\eta$ ) are appropriately resolved (minimum of 15 and 1.1 grid points in  $\delta_{th}$  and  $\eta$ , respectively). Turbulent inflow boundary with specified density, velocity and species has been imposed at the left-hand  $x_1$  boundary and a partially non-reflective outflow boundary condition had been specified at the right-hand  $x_1$  boundary. Periodic boundary conditions have been imposed on all other boundaries. The current simulations have been setup following the methodology detailed by Minamoto et al. [4] and Doan et al. [5]. The thermochemical conditions in the unburned gas, including the mole fractions of the oxidiser stream, unstretched laminar burning velocity and Zeldovich flame thickness ( $\delta_f = \alpha_T / S_L$  where  $\alpha_T$  is the thermal diffusivity of the mixture.) are shown in Table 1. The turbulent conditions chosen for this study are  $u' = 2.0 \text{ m/s}$  and  $\ell_0 = 0.002 \text{ m}$ . These are comparable to those reported by Oldenhof et al. [13]. The mean inflow velocity  $U_{\text{mean}}$  was chosen to be 6.0 m/s. The unburned gas temperature of  $T_r = 1100 \text{ K}$  is also comparable to that used in the experimental investigation by Ye et al. [14]. The simulations have been run for 2.0 throughpass times (i.e.  $\tau_{\text{sim}} = 2.0L/U_{\text{mean}}$ ), which amounts to 6.67 initial eddy turn over times.

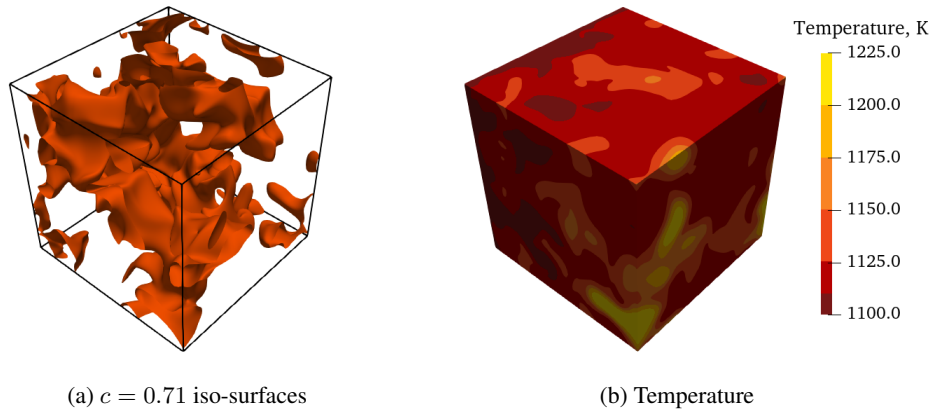
### 4 Results and Discussion

The instantaneous views of  $c = 0.71$  iso-surfaces for the case HM-A are shown in Fig. 1a. The value  $c = 0.71$  corresponds to the maximum heat release for the unstretched laminar premixed flame used to initialise case HM-A (LM-A), and thus it can be considered to represent the flame surface. Fig. 1a shows the distributed nature of the flame in MILD combustion as observed in OH-PLIF visualisations

Table 1: DNS initial conditions for MILD combustion. Values with \* were calculated at  $\langle \phi \rangle = 0.8$ .

Case	$X_{O_2,2}$	$X_{CO_2,2}$	$X_{H_2O,2}$	$\phi$	$S_L$ [m/s]	$\delta_f$ [m]	$l_c/l_0$	$l_\phi/l_c$
HM-A	0.045	0.097	0.112	0.8	0.420	$4.55 \times 10^{-4}$	1.225	-
HM-B	0.030	0.106	0.122	0.8	0.246	$7.84 \times 10^{-4}$	1.225	-
IM-A	0.045	0.097	0.112	0.3 - 1.3	0.420*	$4.55 \times 10^{-4}$ *	1.225	1.34

by Plessing et al. [2]. The figure also shows a considerable amount of flame-self interactions at this  $c$  iso-surface. Fig. 1b shows the temperature variations in case HM-A. Only a modest increase in temperature through the domain is reported, which is consistent with the expectations in MILD combustion [4].

Figure 1: The iso-surfaces at  $c = 0.71$  and the temperature field for case HM-A.

The mean values of the normalised SDF conditioned upon  $c$  are shown in Fig. 2. Here  $\delta_\ell = 1/\max(|\nabla c|_L)$ . Since the flamelet thickness is proportional to the inverse of the maximum of  $|\nabla c| \times \delta_\ell$  conditioned on  $c$ , the lower values of  $\langle |\nabla c| \rangle_c$  (where  $\langle \dots \rangle_c$  is the mean value conditioned upon  $c$ ) are indicative of thickened reaction zone for the turbulent cases. A comparison between Fig. 2b and Fig. 2c shows that increasing the dilution level leads to a slightly thinner reaction zone.

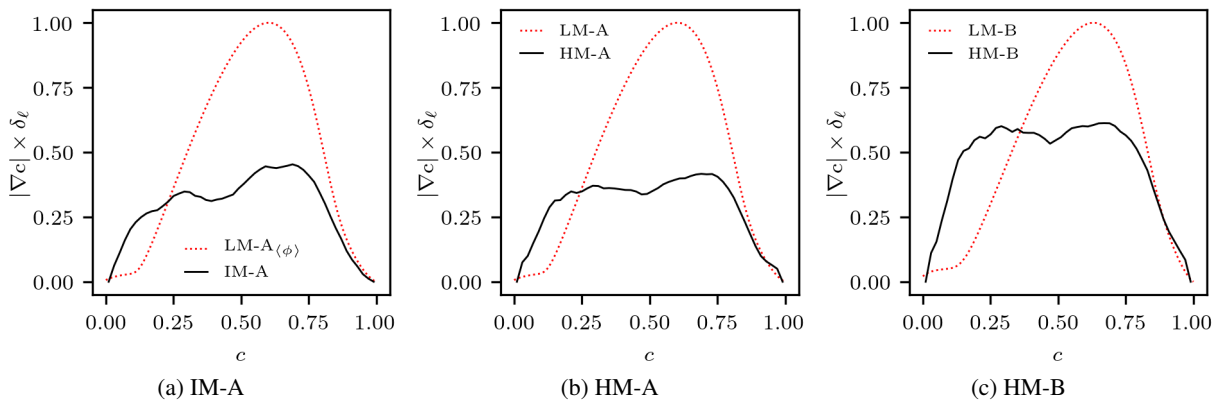


Figure 2: Profiles of the mean values of  $|\nabla c| \times \delta_\ell$  conditioned upon  $c$ . Here "LM" curves refers to the diluted laminar flame used to create the initial MILD field following the methodology by Minamoto et al. [4]

Fig. 3 shows the mean values of the normalised displacement speed  $S_d$  and its components conditioned

upon  $c$ . For all cases, including the inhomogeneous mixture case IM-A, the contribution of the mixture inhomogeneity component  $\langle S_\xi \rangle_c$  remains negligible for all  $c$  values consistent with previous findings for turbulent stratified flames [10]. The reaction contribution in all cases, as manifested in  $\langle S_r \rangle_c$ , remains small for low  $c$  values, but increases in magnitude and assumes peak values towards the burned gas side. Both  $\langle S_t \rangle_c$  and  $\langle S_n \rangle_c$  have approximately the same magnitude and remain positive toward the unburned gas side, but become negative on the burned gas side in all cases, and being the dominant components of  $S_d$  at  $c < 0.5$ , this leads to positive values of  $\langle S_d \rangle_c$  towards the unburned gas side. For the homogeneous cases (HM-A, HM-B),  $\langle S_d \rangle_c$  changes sign at around  $c = 0.5$  which suggests that the leading edge of the flame front propagates into the reactants, whereas the trailing edge retreats into the products indicating local thickening in the reaction zone, as can also be observed from Fig. 2b and Fig. 2c where a local dip in  $\langle |\nabla c| \rangle_c$  profiles occurs at  $c \approx 0.5$ .

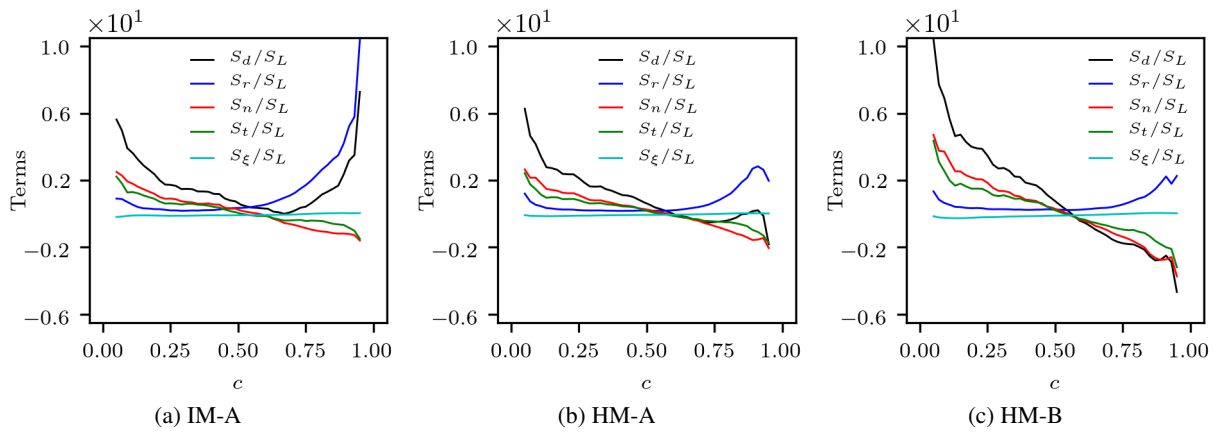


Figure 3: Profiles of the mean values of  $S_d/S_L$  and its components  $S_r/S_L$ ,  $S_n/S_L$ ,  $S_t/S_L$  and  $S_\xi/S_L$  conditioned upon  $c$

Fig. 4 shows the various strain and dilatation rates for all cases. It is clear from the figure that the dilatation rate ( $\nabla \cdot \vec{u}$ ) due to thermal release is negligible in all cases. This suggests that thermal expansion effects are fairly weak in MILD combustion and is consistent with expectations, due to the fairly homogeneous temperature distribution reported in MILD combustion experiments and as shown in Fig. 1b. In all cases, the normal fluid dynamic strain rate ( $a_N$ ) remains negative for all  $c$  values, which indicates that  $\nabla c$  preferentially aligns with the most compressive principal strain rate similar to passive scalar mixing, since the effect of thermal expansion is fairly weak as established before. The negative  $a_N$  give rise to a positive mean value for the tangential fluid-dynamic strain rate ( $a_T = \nabla \cdot \vec{u} - a_N$ ) due to the vanishingly small mean values of  $\nabla \cdot \vec{u}$ , which indicates a flame area generation due to fluid-dynamics straining in all cases. The fluid dynamics strain rates, both normal ( $a_N$ ) and tangential ( $a_T$ ), are small compared to those arising from flame propagation (the normal strain rate  $N_j \partial S_d / \partial x_j$  and the tangential  $2S_d \kappa_m$ ). Thus,  $a_N^{eff}$  and  $a_T^{eff}$  are mostly influenced by the flame propagation induced strain rates. For all cases,  $a_N^{eff}$  maintains mostly positive values for all  $c$  levels. This acts to increase the distance between two adjacent  $c$  iso-surfaces and hence reduces the value of  $|\nabla c|$  and indicates flame thickening. On the other hand, the mostly negative values of  $a_T^{eff}$  indicates a fractional reduction in flame area which could be attributed to strong curvature and flame-self interactions.

## 5 Conclusions

A comparison of the mean behaviour of the magnitude of the reaction progress variable gradient (Surface Density Function, SDF) and its evolution for EGR-type homogeneous and inhomogeneous mixture

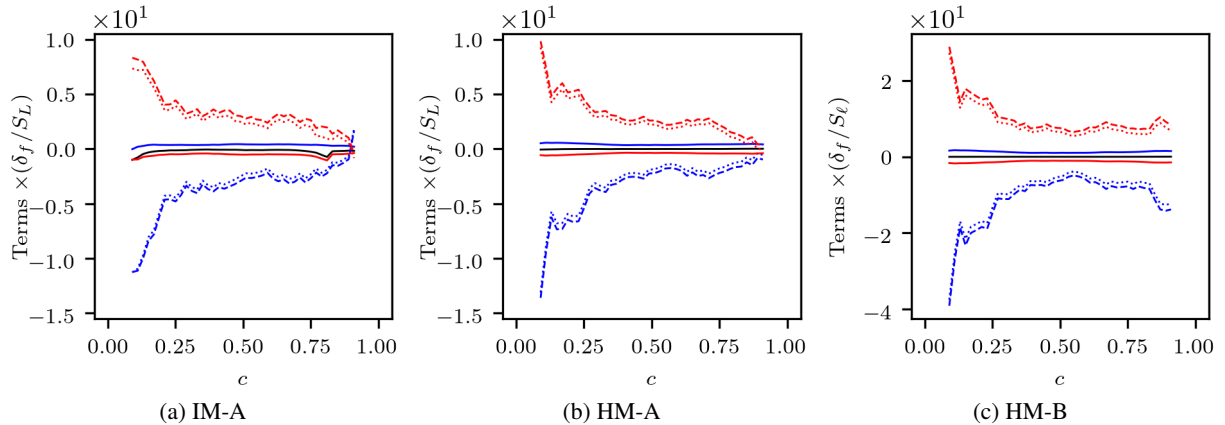


Figure 4: Profiles of the mean values of the various strain rates conditioned upon  $c$ .  $\nabla \cdot \vec{u}$  (—),  $a_T$  (—),  $2S_d \kappa_m$  (- - -),  $a_T^{eff}$  (.....),  $a_N$  (—),  $N_j \partial S_d / \partial x_j$  (- - -) and  $a_N^{eff}$  (.....).

MILD combustion have been conducted using three dimensional DNS with reduced chemical mechanism. It is found that the effect of mixture inhomogeneity was negligible on SDF for the parameters considered here, while increasing the dilution factor gives rise to slightly thinner reaction zone. A generally positive effective normal strain rate could explain the decrease in SDF levels, while the negative effective tangential strain rate indicates a reduction in flame area that could be attributed to flame-self interaction.

### Acknowledgement

The authors are grateful to EPSRC (EP/S025154/1) for the financial support. The computational support was provided by ARCHER2 (EP/R029369/1) and the HPC facility at Newcastle University (Rocket).

### References

- [1] A. Cavaliere and M. de Joannon. Mild Combustion. *Progress in Energy and Combustion Science*, 30(4):329–366, January 2004.
- [2] T. Plessing, N. Peters, and J. G. Wüning. Laser-optical investigation of highly preheated combustion with strong exhaust gas recirculation. *Symposium (International) on Combustion*, 27(2):3197–3204, January 1998.
- [3] İ. B. Özdemir and N. Peters. Characteristics of the reaction zone in a combustor operating at mild combustion. *Experiments in Fluids*, 30(6):683–695, June 2001.
- [4] Y. Minamoto, T. D. Dunstan, N. Swaminathan, and R. S. Cant. DNS of EGR-type turbulent flame in MILD condition. *Proceedings of the Combustion Institute*, 34(2):3231–3238, January 2013.
- [5] N. A. K. Doan, N. Swaminathan, and Y. Minamoto. DNS of MILD combustion with mixture fraction variations. *Combustion and Flame*, 189:173–189, March 2018.
- [6] Y. Minamoto and N. Swaminathan. Subgrid scale modelling for MILD combustion. *Proceedings of the Combustion Institute*, 35(3):3529–3536, January 2015.
- [7] J. Aminian, C. Galletti, S. Shahhosseini, and L. Tognotti. Key modeling issues in prediction of minor species in diluted-preheated combustion conditions. *Applied Thermal Engineering*, 31(16):3287–3300, November 2011.
- [8] F. C. Christo and B. B. Dally. Modeling turbulent reacting jets issuing into a hot and diluted coflow. *Combustion and Flame*, 142(1):117–129, July 2005.
- [9] R. W. Bilger. The structure of turbulent nonpremixed flames. *Symposium (International) on Combustion*, 22(1):475–488, January 1989.
- [10] S. P. Malkeson and N. Chakraborty. Statistical Analysis of Displacement Speed in Turbulent Stratified Flames: A Direct Numerical Simulation Study. *Combustion Science and Technology*, 182(11-12):1841–1883, October 2010.
- [11] C. Dopazo, L. Cifuentes, J. Martin, and C. Jimenez. Strain rates normal to approaching iso-scalar surfaces in a turbulent premixed flame. *Combustion and Flame*, 162(5):1729–1736, May 2015.
- [12] S. Liu, J. C. Hewson, J. H. Chen, and H. Pitsch. Effects of strain rate on high-pressure nonpremixed n-heptane autoignition in counterflow. *Combustion and Flame*, 137(3):320–339, May 2004.
- [13] E. Oldenhof, M. J. Tummers, E. H. van Veen, and D. J. E. M. Roekaerts. Role of entrainment in the stabilisation of jet-in-hot-coflow flames. *Combustion and Flame*, 158(8):1553–1563, August 2011.
- [14] J. Ye, P. R. Medwell, M. J. Evans, and B. B. Dally. Characteristics of turbulent n-heptane jet flames in a hot and diluted coflow. *Combustion and Flame*, 183:330–342, September 2017.